This is an author-created, un-copyedited version of an article accepted for publication in The Astrophysical Journal.
Preprint typeset using LaTeX style emulateapj v. 08/13/06

THE DUST-SCATTERING X-RAY RINGS OF THE ANOMALOUS X-RAY PULSAR 1E 1547.0–5408

A. Tiengo,[1] G. Vianello,[1] P. Esposito,[1,2] S. Mereghetti,[1] A. Giuliani,[1] E. Costantini,[3] G. L. Israel,[4] L. Stella,[4] R. Turolla,[5,6] S. Zane,[6] N. Rea,[7,8] D. Götz,[9] F. Bernardini,[4] A. Moretti,[10] P. Romano,[11] M. Ehle,[12] and N. Gehrels[13]

Received 4 November 2009; accepted 18 December 2009

ABSTRACT

On 2009 January 22 numerous strong bursts were detected from the anomalous X-ray pulsar 1E 1547.0–5408. *Swift*/XRT and *XMM-Newton*/EPIC observations carried out in the following two weeks led to the discovery of three X-ray rings centered on this source. The ring radii increased with time following the expansion law expected for a short impulse of X-rays scattered by three dust clouds. Assuming different models for the dust composition and grain size distribution, we fit the intensity decay of each ring as a function of time at different energies, obtaining tight constrains on the distance of the X-ray source. Although the distance strongly depends on the adopted dust model, we find that some models are incompatible with our X-ray data, restricting to 4–8 kpc the range of possible distances for 1E 1547.0–5408. The best-fitting dust model provides a source distance of 3.91 ± 0.07 kpc, which is compatible with the proposed association with the supernova remnant G 327.24–0.13, and implies distances of 2.2 kpc, 2.6 kpc and 3.4 kpc for the dust clouds, in good agreement with the dust distribution inferred by CO line observations towards 1E 1547.0–5408. However, dust distances in agreement with CO data are also obtained for a set of similarly well-fitting models that imply a source distance of ∼5 kpc. A distance of ∼4–5 kpc is also favored by the fact that these dust models are already known to provide good fits to the dust-scattering halos of bright X-ray binaries. Assuming $N_{\rm H} = 10^{22}$ cm^{-2} in the dust cloud responsible for the brightest ring and a bremsstrahlung spectrum with $kT = 100$ keV, we estimate that the burst producing the X-ray ring released an energy of 10^{44-45} erg in the 1–100 keV band, suggesting that this burst was the brightest flare without any long-lasting pulsating tail ever detected from a magnetar.

Subject headings: dust, extinction — stars: neutron — X-rays: individual (1E 1547.0–5408) — X-rays: stars

1. INTRODUCTION

Soft X-rays are efficiently scattered at small angles by interstellar dust grains. This effect, as predicted by Overbeck (1965) and observationally confirmed by Rolf (1983), is responsible for the presence of X-ray scattering halos around several bright X-ray sources. The X-ray scattering cross section depends on the grain properties, and the observed radial distribution of the photons scattered in the halo also depends on the positions of the scattering grains along the line of sight. Therefore, the study of the energy-dependent radial profile of the X-ray halos gives useful information on the dust grain size, composition, and spatial distribution (see e.g. Predehl & Schmitt 1995).

Scattered X-rays are delayed with respect to direct ones, owing to their longer path length from the source to the observer. In the case of variable sources, these delays give rise to time-dependent effects on the halos properties, that can be used, if the dust spatial distribution is known, to constrain the source distance (Trümper & Schönfelder 1973). This method was applied for the first time to constrain the distance of the X-ray binary Cyg X-3 (Predehl et al. 2000).

An interesting situation occurs when the dust is concentrated only in a thin layer and the X-ray emission has a short duration. In this case the halo appears as a X-ray ring with increasing radius, because only the photons scattered at a well determined angle are detected at a given time. Such "expanding rings" (or "light echoes") have been observed to date in a handful of gamma-ray bursts (GRBs) and by measuring their expansion rate it has been possible to derive accurate distances of Galactic dust clouds (Vianello et al. 2007 and references therein).

Here we report on the discovery of dust scattering rings around the Galactic source 1E 1547.0–5408 (Tiengo et al. 2009). 1E 1547.0–5408 belongs to the small class of anomalous X-ray pulsars (AXPs), which, together with

[1] INAF/Istituto di Astrofisica Spaziale e Fisica Cosmica - Milano, via E. Bassini 15, 20133 Milano, Italy; tiengo@iasf-milano.inaf.it
[2] INFN - Istituto Nazionale di Fisica Nucleare, Sezione di Pavia, via A. Bassi 6, 27100 Pavia, Italy
[3] SRON, Netherlands Institute for Space Research, Sorbonnelaan 2, 3584 CA Utrecht, The Netherlands
[4] INAF/Osservatorio Astronomico di Roma, via Frascati 33, 00040 Monteporzio Catone, Italy
[5] Università degli Studi di Padova, Dipartimento di Fisica, via F. Marzolo 8, 35131 Padova, Italy
[6] University College London, Mullard Space Science Laboratory, Holmbury St. Mary, Dorking, Surrey RH5 6NT, UK
[7] Institut de Ciències de l'Espai (CSIC–IEEC), Campus UAB, Facultat de Ciències, Torre C5-parell, 08193 Barcelona, Spain
[8] University of Amsterdam, Astronomical Institute Anton Pannekoek, Kruislaan 403, 1098 SJ Amsterdam, The Netherlands
[9] CEA Saclay, DSM/Irfu/Service d'Astrophysique, Orme des Merisiers, Bât. 709, 91191 Gif-sur-Yvette, France
[10] INAF/Osservatorio Astronomico di Brera, via E. Bianchi 46, 23807 Merate, Italy
[11] INAF/Istituto di Astrofisica Spaziale e Fisica Cosmica - Palermo, via U. La Malfa 153, 90146 Palermo, Italy
[12] *XMM-Newton* Science Operations Centre, ESAC, ESA, P.O. Box 78, 28691 Villanueva de la Cañada, Spain
[13] NASA Goddard Space Flight Center, Greenbelt, Maryland 20771, USA

the soft gamma-ray repeaters (SGRs) are thought to be magnetars, i.e. isolated neutron stars powered by the energy stored in their extremely strong magnetic field (see Mereghetti 2008 for a recent review). These sources are characterized by the sporadic emission of very bright, short bursts, reaching peak luminosities above $\sim 10^{46}$ erg s^{-1} in the extreme cases known as giant flares. In 2008 October 1E 1547.0–5408 emitted several short bursts and its X-ray flux increased significantly (Israel et al. 2009). No further bursts were reported until 2009 January 22, when the source started a new period of much stronger bursting activity (Mereghetti et al. 2009). This prompted the follow-up X-ray observations that led to the discovery of the three dust scattering rings discussed here.

The paper is organized as follows. In Section 2 we briefly review some properties of the X-ray dust scattering process that will be used in our analysis of the *Swift* and *XMM-Newton* observations described in Section 3. From the expansion rate of the three dust rings we could establish that they originate from the scattering of the same event in three dust layers at different distances (Section 4.1). While this result is independent on the dust properties, the estimate of the distance by modeling the rings intensity (Section 4.2) requires the knowledge of the X-ray scattering differential cross section, hence it depends on the assumed properties of the dust. We found that only a subset of the different dust models that we explored can give satisfactory fits (Section 5.1). The possible distances for 1E 1547.0–5408 from the best-fitting models span a large range of values (Section 5.2), but this can be restricted based on independent information on the gas distribution in the Galaxy (Section 5.3).

2. X-RAY DUST SCATTERING RINGS

The theory of X-ray scattering by interstellar dust grains has been reviewed in several articles (e.g. Mauche & Gorenstein 1986; Mathis & Lee 1991; Smith & Dwek 1998; Draine 2003). Here we remind only a few properties that are relevant to our analysis of the dust scattering rings detected around 1E 1547.0–5408.

Let us consider a source at distance d emitting a short burst of X-ray radiation that is scattered by a thin layer of dust at distance $d_{\rm dust}$. The photons scattered at larger angles reach the observer later because of their longer optical path. Thus the scattering halo appears as a narrow ring centered at the source position and with angular size increasing with time. Considering that the involved angles are small (typically less than 10 arcmin), the ring angular radius $\theta(t)$ is easily derived by simple geometrical considerations giving:

$$\theta(t) = \left[\frac{2c}{d}\frac{(1-x)}{x}(t-t_0)\right]^{1/2} \quad (1)$$

where $x = d_{\rm dust}/d$, c is the speed of light and t_0 is the time at which unscattered photons are detected (in the following called burst time). The photons scattering angle θ_s is related to the ring size by:

$$\theta \approx (1-x)\theta_s \ . \quad (2)$$

If the dust is in our Galaxy and the source is at cosmological distances, as in the case of GRBs, these relations simplify to $\theta(t) = [2c(t-t_0)/d_{\rm dust}]^{1/2}$ and $\theta = \theta_s$, thus the dust distance can be directly derived only from the ring expansion rate. For Galactic sources, instead, both d and $d_{\rm dust}$ can be obtained only if the parameter x is independently measured. This can be done with an analysis of the intensity evolution of the rings as a function of the energy and of the ring radius. In fact, the scattering differential cross-section depends on the grain size and composition, and it rapidly decreases with energy and scattering angle (see e.g. Mauche & Gorenstein 1986). This means that, at any given energy, the ring intensity decrease with the scattering angle is univocally determined by the dust composition and grain size distribution. Since the observed ring radius is related to the scattering angle by equation [2], the parameter x, and therefore the distance of the source and of the dust layer, can be obtained by fitting the energy-resolved intensity decay of an expanding ring at different times. This method is analogous to the analysis of the halo profiles of persistent X-ray sources (see e.g. Predehl & Schmitt 1995), but it has the advantage that the dust distribution along the line of sight is known and the radiation scattered by each dust cloud can be analyzed separately.

For the following analysis it is useful to define an expansion coefficient $K = [19.84(1-x)/(xd)]^{1/2}$. Equation [1] can then be written as

$$\theta(t) = K(t-t_0)^{1/2}, \quad (3)$$

where θ is in arcmin, t in days, and d in kiloparsecs.

Assuming the Rayleigh-Gans approximation (Smith & Dwek 1998), the single-scattering halo profile (expressed in erg cm^{-2} s^{-1} keV^{-1}) predicted for a burst of fluence $F_{\rm X}$ (in erg cm^{-2} keV^{-1}) scattered by grains with size distribution $n(a)$ (dust grains with radius a per hydrogen atom) is (Mathis & Lee 1991):

$$I(\theta, E) = 3.6{\times}10^{-5}\left(\frac{19.84 + K^2 d}{K\ d}\right)^2 N_{\rm H} F_{\rm X} \int {\rm d}a\ n(a)\frac{{\rm d}\sigma}{{\rm d}\Omega} \quad (4)$$

where $N_{\rm H}$ is the hydrogen column density in the dust cloud, $\frac{{\rm d}\sigma}{{\rm d}\Omega} = 1.1(\frac{\rho}{3})^2 a^6 \Phi^2(\theta, E, a, K, d)$ cm^2 is the dust scattering cross-section, ρ is the density (in g cm^{-3}) of each dust component and $\Phi(\theta, E, a, K, d)$ is the form factor. In our case the Rayleigh-Gans approximation is appropriate, since in the following analysis this formula will be applied in the energy range where it is valid ($E > 1.5$ keV). On the other hand, a Gaussian approximation of the form factor is often adopted, but we used the exact formula for spherical uncoated grains (equations [2.4] and [2.5] in Mathis & Lee 1991), since we have verified that in our case the approximation is not accurate enough at large angles and at the highest energies.

Many dust models, with different compositions and grain size distributions, have been proposed and tested against multiwavelength observational data. Weingartner & Draine (2001, WD01) derived a model of dust composed of carbonaceous grains (polycyclic aromatic hydrocarbons at the smallest sizes and graphite for larger grains, which are the responsible for the scattering at X-rays) and amorphous silicate grains. Zubko et al. (2004) proposed 15 dust models, characterized by different abundances of the interstellar medium (B stars, F and G stars, or solar), by the possible presence of composite dust (in addition to bare grains) and by the form

TABLE 1
Observations of 1E 1547.0–5408.

Obs.ID	Start time (MJD)	End time (MJD)	Instrument	Exp./mode[a] (s)
00340573000	54853.438	54853.464	*Swift*/XRT	1967/WT
00340573001	54853.505	54853.531	*Swift*/XRT	2204/WT
00340573001	54853.572	54853.587	*Swift*/XRT	1288/WT
00340573001	54853.639	54853.656	*Swift*/XRT	1432/WT
00340573001	54853.706	54853.722	*Swift*/XRT	1373/WT
00340923000	54854.642	54854.661	*Swift*/XRT	1658/PC
00030956031	54855.262	54855.385	*Swift*/XRT	2560/PC
00341055000	54856.132	54856.259	*Swift*/XRT	3999/PC
00341114000	54856.918	54857.012	*Swift*/XRT	4562/PC
00030956032	54858.063	54858.344	*Swift*/XRT	6182/PC
00030956033	54859.210	54859.417	*Swift*/XRT	4508/PC
00030956034	54859.951	54860.216	*Swift*/XRT	6416/PC
0560181101	54865.768	54866.422	*XMM*/PN	48626/FF
0560181101	54865.753	54866.424	*XMM*/M1	57040/FF
0560181101	54865.753	54866.424	*XMM*/M2	57080/FF

[a]The time resolutions of the operating modes are: XRT Windowed Timing (WT): 1.766 ms; XRT Photon Counting (PC): 2.507 s; PN Full Frame (FF): 73 ms; MOS Full Frame (FF): 2.6 s.

of the bare carbon (graphite, amorphous carbon, or no carbon).

Besides the WD01 model and the 15 models of Zubko et al. (2004), we also tried a simple idealized model, consisting of a single component of dust grains with a power-law size distribution $n(a) \propto a^{-\alpha}$, defined between $a_{\rm min}$ and $a_{\rm max}$ (see e.g. Mathis et al. 1977).

3. OBSERVATIONS

The 2009 January outburst of 1E 1547.0–5408 was extensively followed by the *Swift* satellite with the X-Ray Telescope (XRT; Burrows et al. 2005) operated either in Windowed Timing (WT) mode, characterized by a high time resolution but only mono-dimensional (1D) imaging, or in Photon Counting (PC) mode, where bi-dimensional (2D) imaging of the 10′ radius field of view is available. We used 5 observations in WT mode[14] and 7 observations in PC mode (see Table 1). After 2009 January 30 the rings became too dim to be detected by the *Swift*/XRT instrument. We therefore requested a 50 ks long observation with *XMM-Newton*, that was performed on 2009 February 3–4[15] and allowed us to detect the faint rings thanks to the great sensitivity and large field of view of the EPIC instrument. EPIC is composed of a PN (Strüder et al. 2001) and two MOS X-ray cameras (Turner et al. 2001), that in this observation were operated in Full Frame mode, with the Thick optical blocking filter.

The *Swift*/XRT data were processed with standard procedures using the FTOOLS task XRTPIPELINE (version 0.11.6). We selected events with grades 0–2 for the WT data and grades 0–12 for the PC data. For the spectral analysis, we used the latest available spectral redistribution matrices (version 11). The *XMM-Newton*/EPIC data were processed using the *XMM-Newton* Science Analysis Software (SAS version 9.0.0) and the most recent calibration files. The standard pattern selection criteria for the EPIC X-ray events (patterns 0–4 for PN and 0–12 for MOS) were adopted. The *XMM-Newton* observation was not contaminated by background flares.

[14] We did not use two WT mode observations obtained earlier (MJD 54853.303 and 54853.397) because at those times the rings were too small to be resolved from the bright central source.

[15] Due to visibility constraints *XMM-Newton* could not observe the source earlier.

4. DATA ANALYSIS AND RESULTS

Figure 1 shows the images of the first XRT observation in PC mode and of the EPIC observation. Three concentric rings, centered at the position of 1E 1547.0–5408, are clearly visible in the images. They could be due to scattering of three bursts by a thin dust layer along the line of sight or by three dust layers scattering the same event.

4.1. *Ring expansion*

To derive the expansion rate of the dust scattering rings we used only the full imaging data, in which the ring radii can be well constrained (7 XRT observations in PC mode and the sum of the three EPIC images). We first cleaned the data by excluding time intervals during which bright bursts from 1E 1547.0–5408 were detected.

We limited the analysis of the XRT data to the 1–6 keV energy range, where the rings are significantly detected. In order to avoid contamination by spatially variable emission lines in the instrumental background, the analysis of the PN and MOS data was restricted to the 1.6–6 keV and 1.9–6 keV range, respectively. In EPIC, we removed the point sources detected in the field and the out-of-time PN events from the bright central source. For each data set we extracted a radial profile centered at the position of 1E 1547.0–5408, as derived with a standard centroid search algorithm in each observation. The number of counts in each radial bin was normalized to the enclosed area and divided by the corresponding average exposure time derived from the exposure map, in order to correct the observed profile for the vignetting, the dead detector areas, and the excluded regions. The resulting radial profiles, where the peaks due to three rings are clearly visible, are shown in Figure 2.

The point-spread functions (PSFs) of *Swift*/XRT (Moretti et al. 2005) and *XMM-Newton*/EPIC (Read 2004) are well modeled by a King profile. We verified through simulations that the radial profile of a thin ring broadened by a PSF with a King profile is well fit by a Lorentzian function. Since the rings slightly expand during each observation, their profile is expected to be asymmetric, but we verified that a fit with a Lorentzian is still a good approximation due to the relatively short duration of our observations. Therefore we fit the radial profiles with a model consisting of the sum of a King profile (to account for the central point source[16]), three Lorentzian components (corresponding to the three rings) and a constant (representing the background).

The angular size of the three rings, as obtained from the best-fit values of the Lorentzian centroids, is plotted as a function of time in Figure 3. We used equation [3] to fit the size evolution of the three rings, with K and t_0 as free parameters, and obtained good χ^2 values (6.2/6 degrees of freedom [dof], 5.1/6 dof and 0.8/6 dof). The

[16] The derived parameters indicated also the presence of an additional extended component; its possible origin is discussed in Section 5.3

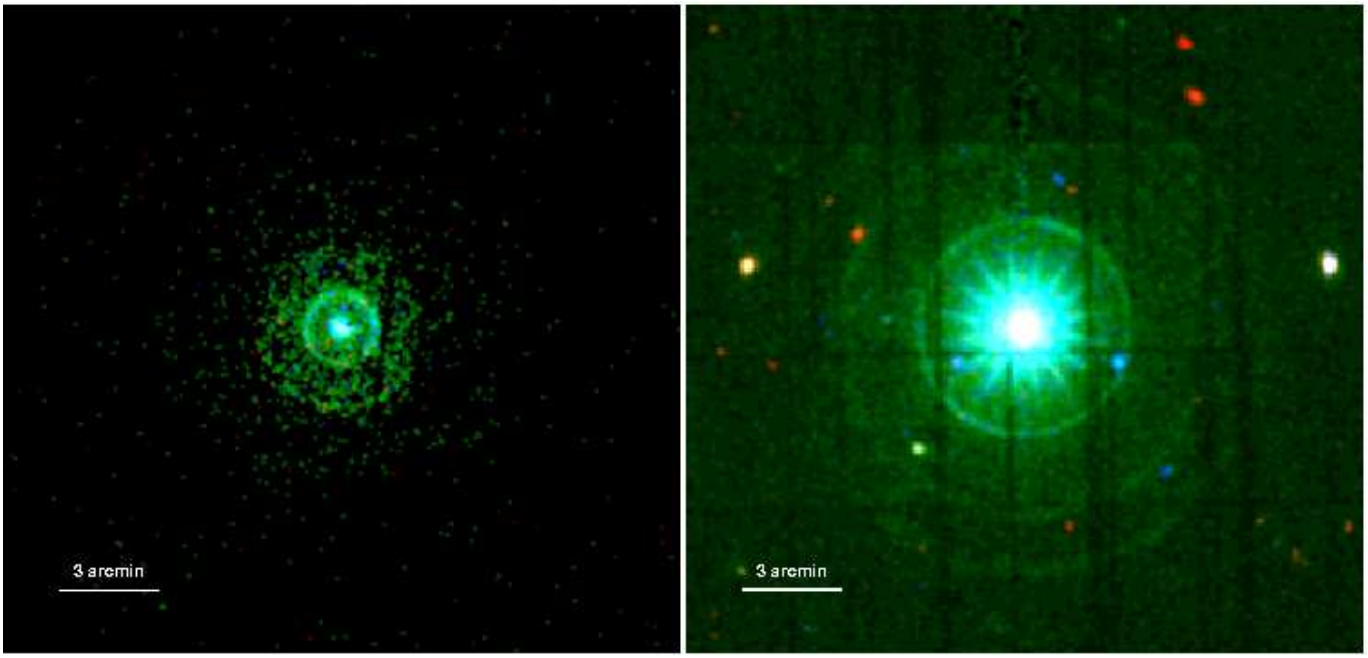

FIG. 1.— The first *Swift*/XRT image of the rings obtained in Photon Counting mode (left panel) and the *XMM-Newton*/EPIC image obtained 12 days later (right panel). The images are slightly smoothed and the red, green and blue colors correspond to the 0.5–1.4 keV, 1.6–4 keV and 4–7 keV energy bands, respectively.

best-fit t_0 values for the three rings resulted consistent with a single burst time, while three significantly different values for K were found. This means that the rings were produced by the scattering of the same burst (or of a series of bursts occurring within a short time interval) by three dust layers at different distances.

The derived t_0 values are compatible with the short time interval from 6:43 to 6:51 UT of 2009 January 22, in which the highest bursting activity was seen during a long, uninterrupted observation obtained with the Anti-Coincidence Shield (ACS) of the Spectrometer on *INTEGRAL* (SPI) instrument (Mereghetti et al. 2009). Among the several tens of short bursts seen in this interval, two events were outstanding for their exceptional brightness: a burst at 6:45:14 UT lasting ∼1.5 s and a longer event that occurred at 6:48:04 UT. The latter burst consisted of an initial bright spike, lasting 0.3 s, followed by a tail pulsed at the 2.1 s rotation period of 1E 1547.0–5408.[17] Both events saturated the ACS and the first one saturated also the detector on the *RHESSI* satellite (Bellm et al. 2009). Therefore it is not possible to establish which of the two bursts had a higher fluence in the soft X-ray range and caused the scattering rings. Due to the small time delay between these two events, all our analysis and results of the next section do not depend significantly on which of these burst was the origin of the rings (in fact it is also possible that both events contributed to the observed scattered X-rays). In the following we will assume that the observed rings were produced by the first burst and define $T_0 = 54853.28141$ MJD = 2009 January 22 at 6:45:14 UT.

The fits result gave $t_{0,1} = T_0 - 1000 \pm 1100$ s, $t_{0,2} = T_0 - 4000 \pm 1900$ s, and $t_{0,3} = T_0 + 300^{+1100}_{-1600}$ s (all the errors are at 1 σ). Fitting jointly the three rings imposing a common t_0, we obtain a 90% confidence interval $T_0 - 2100$ s $< t_0 < T_0 + 700$ s. Finally, by fixing $t_0 = T_0$, the fit yields the expansion coefficients $K_1 = 0.8845 \pm 0.0008$, $K_2 = 1.553 \pm 0.003$, and $K_3 = 2.000 \pm 0.002$ (χ^2/dof=17.2/21).

[17] The other pulsed burst detected at 8:17:29 UT (Mereghetti et al. 2009) is incompatible with the possible values for t_0 and therefore cannot be the origin of the X-ray rings.

4.2. *Spectra and radial profiles*

Here we describe our analysis of the energy-dependent halo profiles, i.e. the spectra $I(E, \theta)$ of the three rings at the different angles θ from the source direction. In fact, having already determined the expansion rate, for any given dust scattering model, $I(E, \theta)$ depends only on the source distance, column density $N_{\rm H}$, and fluence $F_{\rm X}(E)$ of the primary radiation (see equation 4). By simultaneously fitting $I(E, \theta)$ for the three rings we will derive some information on these quantities.

While the relative optical depth of the three dust layers is set by the relative intensity of the three rings, their absolute values are unknown because the burst fluence $F_{\rm X}(E)$ in the soft X-ray band was not directly measured. In the following analysis we fixed the column density of the dust cloud producing the innermost and brightest ring at $N_{\rm H1} = 10^{22}$ cm^{-2}. This value was chosen considering that the total $N_{\rm H}$ along the line of sight derived from the X-ray spectrum of 1E 1547.0–5408 is $\sim 3 \times 10^{22}$ cm^{-2} (Halpern et al. 2008). The burst fluence $F_{\rm X}(E)$ that we will derive from the fits of $I(E, \theta)$ depends on the assumed value $N_{\rm H1}$. Also the column densities obtained for the two other clouds, $N_{\rm H2}$ and $N_{\rm H3}$, will be relative to $N_{\rm H1}$. However, it is important to note that the derived distances do not depend on $N_{\rm H1}$ since, for any fixed dust model, they are determined only by the relative intensity of the rings at different times and energies (see equation [3]).

The extraction of the ring spectra by selecting annular regions (in the data sets with 2D images) is hampered

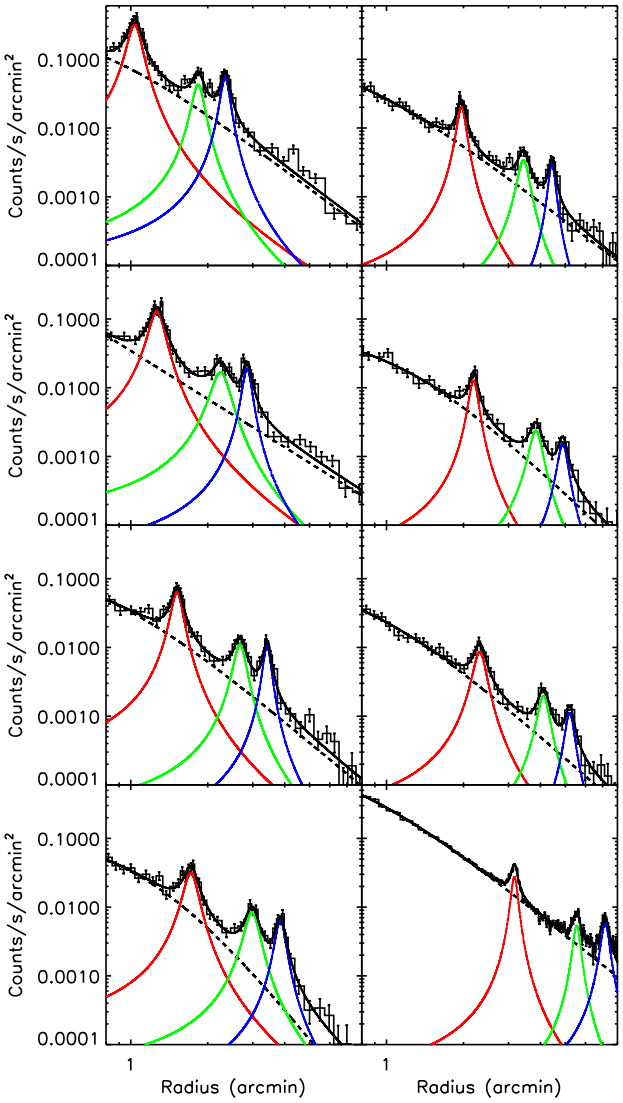

FIG. 2.— Exposure-corrected radial profiles of the seven *Swift*/XRT observations in PC mode and of the *XMM-Newton*/EPIC observation. The model is composed by a King profile (dashed line) plus three Lorentzian components (red, green, and blue). A spatially uniform background has been subtracted.

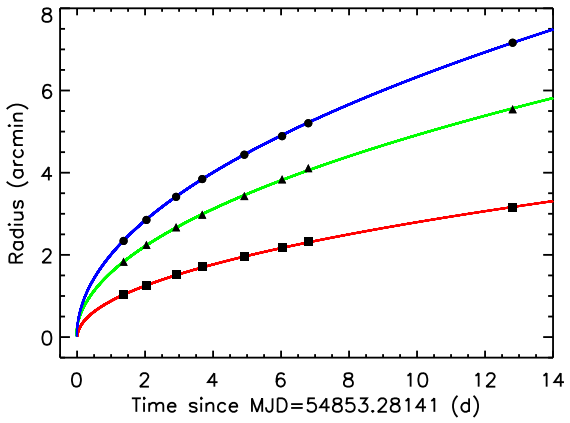

FIG. 3.— Expansion of the three dust scattering rings as observed by *Swift*/XRT in PC mode and *XMM-Newton*/EPIC. The lines show the best fit model $\theta(t) = K(t - t_0)^{1/2}$ for the three rings. The error bars on the ring radii are not shown since they are much smaller than the symbols.

by the spatial proximity of the three rings and by the contamination from the bright central point source and from the diffuse halo. Therefore, we followed a different approach to obtain the background-subtracted spectra of the rings: we derived the number of counts per energy bin by fitting the energy resolved radial profiles of every observation. In order to properly take into account for all the instrumental and systematic effects, we did not use an analytic expression (as done in the previous section), but we resorted to detailed simulations to derive the expected radial profile of each of the following five components: the three rings, the central source and the background.

For each observation listed in Table 1 and for each component separately, we simulated a 2-D image taking into account the effect of the instrumental PSF. A sufficiently large number of photons was generated in order to minimize statistical uncertainties. The rings expansion was simulated based on the real observation plan and on the expansion law derived above.[18] The resulting images were convolved with the exposure maps of the corresponding real observations, in order to correct for the vignetting, detector defects and gaps and, in the case of the *XMM-Newton* data, the regions excluded to eliminate the field point sources (and out-of-time events for the PN).

At this point, we produced the radial profiles of the simulated XRT/PC and EPIC images, while for the simulations of the 5 XRT observations in WT mode we projected the images onto the X axis of the XRT CCD. These histograms, with a variable normalization factor, were used to fit the radial profiles and the 1-D WT images observed at the different energies. The ratio between the number of photons in the simulation and the normalization factor (with the statistical error obtained by the fitting procedure) provides the number of photons of the component in the selected energy range. Using this method to extract all the spectra, no PSF correction must be applied to the ancillary response files (ARF), because the PSF profile is integrated over the whole detector plane. Similarly, no corrections for vignetting and chip defects must be applied, because they were already taken into account during the simulation process. The WT spectra of the two outermost rings were excluded from the following analysis because their counts could not be unambiguously separated in the WT profiles.

To properly model the observed X-ray profiles, the addition of a diffuse halo component was also required. Since it has a non-uniform spatial distribution that we are not able to model *a priori*, we described it with an analytical function convolved with the exposure map: for the 2-D data we used a King profile centered on 1E 1547.0–5408, while for the WT data we used a King function convolved with a constant gradient along the

[18] The two outer rings in the EPIC data are significantly broader than predicted by the PSF and the ring expansion. We could adequately model their profiles adopting a 200 pc thickness for the corresponding dust layers. Although this effect is detectable only in the EPIC images, we introduced it also in the simulations of the two outer rings for all the *Swift* observations.

TABLE 2
BEST-FIT PARAMETERS OF THE HALO PROFILES WITH DIFFERENT DUST MODELS.

Dust model	Distance (kpc)	$\frac{N_{H2}}{N_{H1}}$	$\frac{N_{H3}}{N_{H1}}$	χ^2_{red}/dof
bare-gr-b	3.91±0.07	0.24±0.01	0.27±0.01	0.77/193
bare-gr-s	4.76±0.08	0.25±0.01	0.30±0.01	0.79/193
bare-gr-fg	4.86±0.09	0.25±0.01	0.30±0.01	0.81/193
comp-gr-b	5.22±0.10	0.26±0.01	0.31±0.01	0.85/193
power-law[a]	5.40±0.13	0.26±0.01	0.32±0.01	0.86/192
comp-gr-fg	6.95±0.13	0.28±0.01	0.35±0.01	1.05/193
power-law[b]	4.86±0.08	0.25±0.01	0.29±0.01	1.09/193
comp-gr-s	7.71±0.14	0.29±0.01	0.37±0.01	1.10/193
power-law[c]	6.05±0.10	0.27±0.01	0.33±0.01	1.12/193
power-law[d]	7.33±0.13	0.28±0.01	0.36±0.01	1.14/193
WD01	6.91±0.12	0.27±0.01	0.34±0.01	1.27/193
comp-nc-b	11.83±0.24	0.33±0.01	0.46±0.01	1.33/193
bare-ac-s	5.74±0.10	0.26±0.01	0.31±0.01	1.36/193
bare-ac-b	4.83±0.08	0.24±0.01	0.28±0.01	1.37/193
bare-ac-fg	5.85±0.10	0.26±0.01	0.31±0.01	1.44/193
comp-ac-b	8.37±0.16	0.27±0.01	0.36±0.01	1.52/193
comp-ac-s	9.24±0.17	0.29±0.01	0.39±0.01	1.55/193
comp-ac-fg	8.14±0.15	0.28±0.01	0.36±0.01	1.73/193
comp-nc-s	10.17±0.19	0.29±0.01	0.40±0.02	1.81/193
comp-nc-fg	10.36±0.24	0.30±0.01	0.41±0.01	1.87/193

[a]Power-law grain size distribution $a^{-\alpha}$ with $\alpha = 3.66 \pm 0.02$, $a_{min} = 0.0003$ μm and $a_{max} = 0.3$ μm.
[b]Power-law grain size distribution $a^{-\alpha}$ with $\alpha = 3.5$, $a_{min} = 0.0003$ μm and $a_{max} = 0.25$ μm.
[c]Power-law grain size distribution $a^{-\alpha}$ with $\alpha = 3.5$, $a_{min} = 0.0003$ μm and $a_{max} = 0.3$ μm.
[d]Power-law grain size distribution $a^{-\alpha}$ with $\alpha = 3.5$, $a_{min} = 0.0003$ μm and $a_{max} = 0.35$ μm.

X axis because we detected an asymmetry of the diffuse halo.

With the procedure described above we obtained the rings spectra for each observation. We then fitted these spectra with a phenomenological model (an absorbed power-law) in order to obtain the ring's specific intensities as a function of θ at seven energy values between 2 and 7 keV. As an example we show in Figure 4 the results for 2, 3, 4 and 5 keV, where the data points of the three rings are indicated by different colors. The 21 radial profiles (seven energies times three rings) were simultaneously fitted with the model of equation [4] for the different dust compositions and grain size distributions described in Section 2, yielding the results reported in Table 2. A joint fit is justified by the assumption that the three dust clouds are spatially uniform in the plane of the sky and are made of dust with the same composition and grain size distribution.

It is evident that, although formally acceptable fits were obtained with different dust models and the corresponding errors on the fitted parameters are rather small, there is a wide spread in the derived distances for 1E 1547.0–5408.[19] All the dust models give reasonably similar values for the relative N_H values of the three dust clouds.

5. DISCUSSION

[19] In order to discriminate among these dust models, an independent measure of the distance of the X-ray source or of at least one of the three dust clouds would be required. A robust measure of any of these distances is still lacking, but the currently available constraints are discussed in the next section.

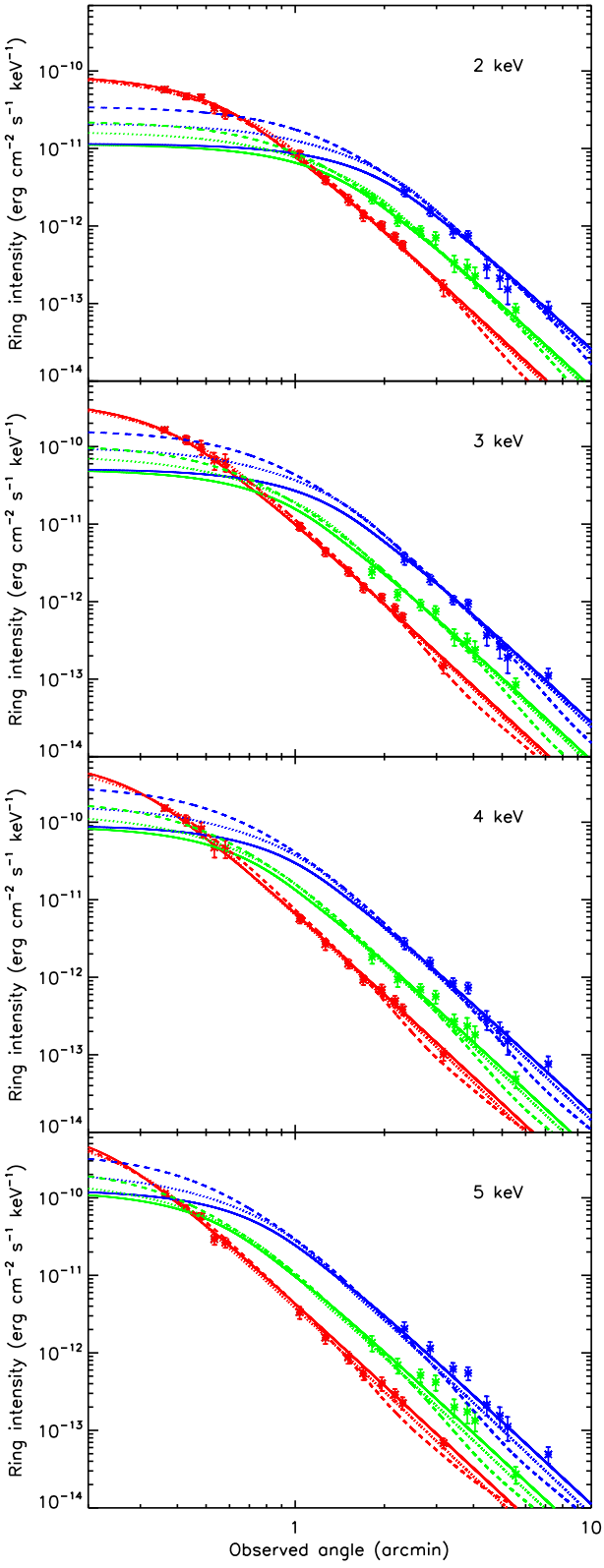

FIG. 4.— Halo profiles at different energies for the three rings. The models are based on the following dust compositions and grain size distributions: WD01 from Weingartner & Draine (2001) (dotted lines), BARE-GR-B (solid lines) and COMP-NC-FG (dashed lines) from Zubko et al. (2004). See Table 2 for the corresponding best-fit parameters.

By measuring the expansion rate of the dust scattering rings seen in X-ray observations of the AXP 1E 1547.0–5408 we established that they were produced by three dust clouds at different distances, and that the most likely origin of the scattered X-rays was the extremely bright burst that occurred on 2009 January 22 at 6:45:14 UT (Mereghetti et al. 2009). With a detailed spatial and spectral analysis of the three X-ray rings we could test different dust models and derive some information on the distance of 1E 1547.0–5408, on the distance and optical depth of the three dust clouds, and on the ∼2–7 keV properties of the burst (that was observed directly only at higher energy). Despite the large systematic uncertainty on the 1E 1547.0–5408 distance, resulting from our ignorance of the actual dust properties, our analysis yielded some results that have implication both for the study of the Galactic dust properties and of 1E 1547.0–5408.

5.1. *Dust models*

The dust models that we adopted are characterized by different cross sections for X-ray scattering. As a consequence the quality of the fits to the energy-dependent angular profiles of the rings is not the same in all models, as demonstrated by the χ^2 values reported in Table 2. It is remarkable that the models giving the best fits, namely the ones containing bare graphite grains and no composite dust, are the same already found to better describe the dust-scattering halos of other Galactic X-ray sources (Smith et al. 2006; Smith 2008; Valencic et al. 2009). On the other hand, the models with no carbon or amorphous carbonaceous grains provide significantly poorer fit to our X-ray data. Within the same class of models, we generally find a better fit for the dust models constructed according to the abundances of B stars. However, since the profiles of the X-ray scattering halos are more sensitive to the dust grain size distribution rather than to its chemical composition, the elemental abundances of the interstellar medium cannot be directly constrained by our analysis.

As can be seen from the examples shown in Figure 4, the models yielding unacceptable fits systematically underestimate the ring flux at high energies and large off-axis angles. This means that such models have a deficit of relatively small grains ($a \sim 0.01$–0.03 μm), which are the most efficient in scattering the harder X-rays and are responsible for the larger scattering angles.

5.2. *Distance of 1E 1547.0–5408 and burst energy*

The distances of 1E 1547.0–5408 derived assuming the different dust models have very small statistical errors, but span a large range of values. In fact the source distance is particularly sensitive to the dimensions of the largest grains, which are mainly responsible for the scattering at the smallest angles of soft X-rays. The largest grains determine the ring fluxes at low energies during the first observations, where we detected most of the scattered photons. The strong dependence of the source distance on the size of the largest dust grains is well demonstrated by our fits with a power-law grain size distribution (see Table 2 for a few examples). Keeping the same power-law index and minimum grain dimension, we found that the source distance is related to the maximum grain radius by $d \propto {a_{\rm max}}^{4/3}$.

All the dust models giving the best fits to the halo profiles yield source distances in the relatively narrow range $d \sim 4$–5 kpc, and, as noted above, they are the most successful also for other Galactic X-ray sources. This distance estimate for 1E 1547.0–5408 agrees with that suggested on the basis of its possible association with the supernova remnant G 327.24–0.13 and a star forming region (Gelfand & Gaensler 2007). A distance of 9 kpc was instead derived from the dispersion measure of the 1E 1547.0–5408 radio pulses (Camilo et al. 2007), assuming the Galactic free electron density model of Cordes & Lazio (2002). This model is known to have an average uncertainty of ∼30%, which, however, can be much larger for individual objects.

The results of our fit give also some constraints on the X-ray properties of the burst that produced the scattering rings. In principle, once the column density in one cloud is fixed, the burst spectrum could be obtained directly from the normalizations of the models fitting the energy-resolved halo profiles. However, due to the limited energy band and the relatively large normalization errors, the broad-band spectral shape of the burst is poorly constrained. Therefore, we adopted for the burst an absorbed bremsstrahlung model with temperature fixed at 30 keV or 100 keV, as suggested by the observations of other magnetar bursts. The corresponding best-fit parameters found for the different dust models are reported in Table 3. The derived fluences vary by a factor ∼3, because the dust scattering efficiency changes in the different models. The table reports also the burst energy in the 1–100 keV energy band, computed with the appropriate source distance resulting from each dust model. The derived values are in the range $\sim 10^{44-45}$ erg, i.e. not far from the energy emitted in the giant flares of SGR 0526–66 (Mazets et al. 1979) and SGR 1900+14 (Hurley et al. 1999). However, we remind that our energy estimate is inversely proportional to the value for the dust optical depth that we have assumed by fixing $N_{\rm H1}$=10^{22} cm^{-2}.

5.3. *Distances and properties of the dust clouds*

The distances of the three dust clouds are related to the expansion coefficients K and the source distance d by $d_{\rm dust} = 19.84\ d/(19.84 + K^2 d)$ kpc. Therefore, for each model of Table 2 we can derive the distances of the three clouds and compare them with independent estimates of the dust distribution in the direction of 1E 1547.0–5408.

In order to obtain the distribution of molecular hydrogen along the line of sight we use the CO observations obtained by the Millimeter-Wave Telescope at the Harvard-Smithsonian Center for Astrophysics (CfA) (Dame et al. 2001). The CO is assumed to be a tracer of molecular hydrogen, through a known ratio (X) between hydrogen density and CO radio emissivity; for this work we assumed $X = 2.3 \times 10^{20}$ cm^{-2} K^{-1} km^{-1} s. The velocity-resolved radio data have been deprojected using the Galactic rotation curve parameterized by Clemens (1985). As shown in Figure 5, the strongest peak of CO emission is located at a distance of ∼3.5 kpc. This value is consistent with the distance of the farthest cloud (producing the innermost and brightest ring) if 1E 1547.0–5408 is at ∼4 kpc, as found with the models that gave the lowest χ^2 in the halo profile fits. In particular, the best fitting model BARE-GR-B gives $d = 3.9$ kpc and

TABLE 3
BEST-FIT PARAMETERS WITH AN ABSORBED BREMSSTRAHLUNG MODEL OF THE BURST UNSCATTERED SPECTRUM.

Dust model	$N_{\rm H}$ ($\rm cm^{-2}$)	kT[a] (keV)	F_{burst}[b] (erg $\rm cm^{-2}$)	E_{burst}[c] (erg)	$\chi^2_{\rm red}$[d]
bare-gr-b	4.5×10^{22}	30	0.0050	1.0×10^{44}	1.02
	4.2×10^{22}	100	0.0050	1.9×10^{44}	0.17
bare-gr-s	4.5×10^{22}	30	0.0039	1.2×10^{44}	0.99
	4.2×10^{22}	100	0.0039	2.2×10^{44}	0.17
bare-gr-fg	4.5×10^{22}	30	0.0038	1.2×10^{44}	1.27
	4.2×10^{22}	100	0.0038	2.2×10^{44}	0.30
comp-gr-b	4.4×10^{22}	30	0.0045	1.6×10^{44}	0.25
	4.2×10^{22}	100	0.0045	3.0×10^{44}	0.23
comp-gr-fg	4.4×10^{22}	30	0.0034	2.2×10^{44}	0.23
	4.2×10^{22}	100	0.0034	4.0×10^{44}	0.70
comp-gr-s	4.4×10^{22}	30	0.0033	2.6×10^{44}	0.31
	4.2×10^{22}	100	0.0033	4.8×10^{44}	1.05
WD01	4.3×10^{22}	30	0.0020	1.3×10^{44}	0.70
	4.1×10^{22}	100	0.0020	2.3×10^{44}	1.82
comp-nc-b	4.5×10^{22}	30	0.0059	1.1×10^{45}	0.96
	4.2×10^{22}	100	0.0059	2.0×10^{45}	0.33
bare-ac-s	4.3×10^{22}	30	0.0036	1.6×10^{44}	0.39
	4.1×10^{22}	100	0.0036	2.9×10^{44}	0.64
bare-ac-b	4.3×10^{22}	30	0.0045	1.4×10^{44}	0.35
	4.1×10^{22}	100	0.0045	2.6×10^{44}	0.76
bare-ac-fg	4.3×10^{22}	30	0.0035	1.6×10^{44}	0.45
	4.1×10^{22}	100	0.0035	2.9×10^{44}	0.83
comp-ac-b	4.8×10^{22}	30	0.0077	7.6×10^{44}	1.93
	4.5×10^{22}	100	0.0077	1.4×10^{45}	0.59
comp-ac-s	4.5×10^{22}	30	0.0041	4.8×10^{44}	0.33
	4.3×10^{22}	100	0.0041	8.7×10^{44}	1.15
comp-ac-fg	4.4×10^{22}	30	0.0042	3.8×10^{44}	0.43
	4.1×10^{22}	100	0.0042	6.8×10^{44}	1.39
comp-nc-s	4.6×10^{22}	30	0.0050	7.2×10^{44}	0.31
	4.4×10^{22}	100	0.0050	1.3×10^{45}	0.28
comp-nc-fg	4.6×10^{22}	30	0.0050	7.4×10^{44}	0.25
	4.3×10^{22}	100	0.0050	1.3×10^{45}	0.54

[a]Fixed.
[b]Observed fluence in the 2–5 keV energy band, assuming $N_{\rm H1} = 10^{22}$ $\rm cm^{-2}$.
[c]Unabsorbed energy emitted in the 1–100 keV energy band, assuming $N_{\rm H1} = 10^{22}$ $\rm cm^{-2}$ and the source distances reported in Table 2.
[d]For 5 dof.

$d_{\rm dust}$ = 3.4, 2.6 and 2.2 kpc for the three clouds (see solid lines in Figure 5). The presence of a large amount of dust at a distance of ∼3.5 kpc in this direction is also confirmed by the analysis of the infrared extinction of the field stars (Marshall et al. 2006).

The relative amount of dust in the three clouds can be inferred by the ratio of their hydrogen column densities, since, for each dust model, we used the same fraction of dust grains per hydrogen atom in the three clouds. All the dust models give similar column density ratios (see Table 2), with the farthest cloud containing ∼2–4 times more dust than each of the other two clouds. This scenario is also compatible with the CO data and a source distance of ∼4 kpc, since the two closest clouds could be the responsible for the lower and broader peak of CO emission detected at a distance of 2–3 kpc (see Figure 5). For larger 1E 1547.0–5408 distances the largest CO emission peak could be associated with one of the closer dust clouds. However, in this case the cloud responsible for the brightest ring would be located at a larger distance, where, based on CO emission data, a smaller amount of dust is expected. In conclusion, it seems that also

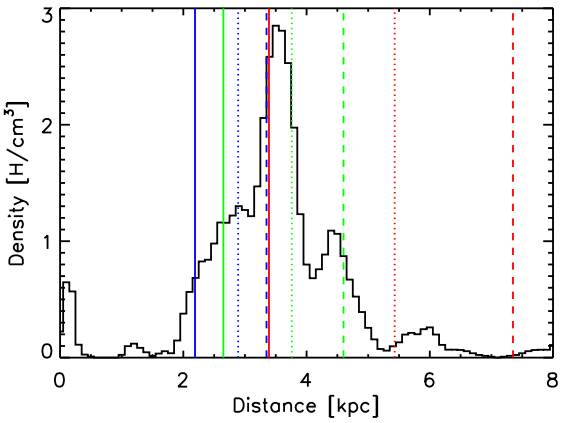

FIG. 5.— Density of molecular hydrogen in the direction of 1E 1547.0–5408, as derived from CO observations. The vertical lines show the inferred distances of the three dust clouds (red, green and blue for the clouds generating the smallest, intermediate and largest ring, respectively) for the following dust models: WD01 from Weingartner & Draine (2001) (dotted lines), BARE-GR-B (solid lines) and COMP-NC-FG (dashed lines) from Zubko et al. (2004). See Table 2 for the corresponding best-fit parameters.

from an analysis of the plausible locations of the three dust clouds, a distance of ∼4 kpc for 1E 1547.0–5408 is favored.

It is reasonable to expect that not all the dust along the line of sight be concentrated in the three clouds responsible for the rings. This is supported by the analysis of the radial profiles discussed in Section 4.2. In fact, in all observations, we obtained best-fit parameters of the King profile different from those expected for a point source, clearly indicating the presence of a further component of diffuse emission around 1E 1547.0–5408. We found that the intensity of this component significantly decreases with time, consistently with its interpretation as scattering of the 1E 1547.0–5408 burst by dust distributed along the whole line of sight. Another possibility is multiple scattering by the three thin dust layers; moreover, some contribution to this halo can come from the dust scattering of the X-ray emission of the other bursts occurring during the source activation and of the persistent X-ray emission of 1E 1547.0–5408.

We finally note that the diffuse X-ray emission recently reported by Vink & Bamba (2009) and interpreted as emission of a pulsar wind nebula powered by 1E 1547.0–5408 and of the supernova remnant G 327.24–0.13 is significantly dimmer than the extended emission (either the expanding rings or diffuse halo) described here.

6. CONCLUSIONS

Three bright X-ray rings were discovered around the anomalous X-ray pulsar 1E 1547.0–5408 after its strong bursting activity of 2009 January 22. Their radii were seen to increase and their flux to decrease with time, as expected for a short burst of X-rays scattered by three thin dust layers. A similar phenomenon had been observed in a few GRBs, but on a much smaller scale: in the best case, the rings around GRB 031203 (Vaughan et al. 2004) were observed by *XMM-Newton* from 5 to 20 hours after burst, but only ∼3,000 ring photons could be collected. The ∼65,000 ring photons we detected for 1E 1547.0–5408 allowed us to carry out a detailed anal-

ysis in which several subtle effects, that could have been neglected with a smaller statistics, had to be carefully taken into account.

Based only on simple, model-independent geometrical considerations, we found that the delayed X-rays seen in the rings were emitted by 1E 1547.0–5408 within the same time interval of the unscattered radiation detected between 6:10 and 6:56 UT of 2009 January 22 in hard X-rays. This short time period includes the phase of highest bursting activity ever observed from this source.

Interesting information on 1E 1547.0–5408 and on the dust clouds producing the X-ray rings could be derived from the analysis of the ring's spectra and intensity evolution. However, this analysis requires the knowledge of the interstellar dust properties affecting the X-ray scattering cross section. We therefore explored the consequences of using different dust models.

The energy released by the event that formed the X-ray scattering rings could be derived from the fit of the halo profiles, that provides at the same time its spectrum and fluence in the 2–5 keV band, and the source distance. Assuming a column density of 10^{22} cm^{-2} for the most distant cloud and a bremsstrahlung spectrum with $kT =$ 30–100 keV, a burst energy between 10^{44} erg and 2×10^{45} erg was derived (in the 1–100 keV range). These values are significantly larger than that in the pulsating tail detected on 2009 January 22 at 6:48 UT ($E \sim 2.4 \times 10^{43} d^2_{10\ \mathrm{kpc}}$ erg; Mereghetti et al. 2009), that therefore cannot account for the rings. More likely candidates are two bright bursts, whose fluence could not be determined because they were so bright to saturate the detectors, and occurred at times compatible with the expansion rate measured for the rings. However, we cannot exclude that the event producing the scattering rings had a very steep spectrum and so dominated the emission at soft X-rays without showing up as an exceptional event at higher energies.

According to our estimate, the energy released by the event that generated the X-ray scattering rings is comparable to that emitted by the giant flares of SGR 0526–66 (Mazets et al. 1979) and SGR 1900+14 (Hurley et al. 1999). These events were followed by pulsating tails lasting several minutes, contrary to the case of 1E 1547.0–5408: the only pulsating tail detected by the continuous *INTEGRAL* ACS observation covering the time interval compatible with the origin of the X-ray rings lasted only 8 seconds (Mereghetti et al. 2009). On the other hand, in case the X-ray scattering rings of 1E 1547.0–5408 were produced by a single short burst, it must have been exceptionally bright, since no other magnetar bursts without any pulsating tail and an emitted energy $>10^{44}$ erg have ever been detected. The intermediate flare emitted by SGR 1627–41 on 1998 June 18 (Mazets et al. 1999) was the former record holder, with $E \sim 10^{43}$ erg (assuming a distance of 11 kpc). We caution that large systematic uncertainties affect our estimate of the emitted energy: the total scattering cross-section and source distance depend on the dust model, the hydrogen column density and dust-to-gas ratio in the dust clouds are only poorly constrained, and the broad band spectrum is inferred from a narrow band X-ray spectrum and in analogy to similar events.

By using several dust models discussed in the literature we showed that only about half of them provide an adequate fit to the three halo profiles at different energies. The best-fitting model (BARE-GR-B in Zubko et al. 2004) yields for 1E 1547.0–5408 a distance of 4 kpc, consistent with the value derived from its association with the SNR G 327.24–0.13 (Gelfand & Gaensler 2007). This model also gives distances for the three dust clouds that are consistent with CO observations in this direction.

Our best fitting dust model is the same that provided the best fits to the halo of GX5–1 (Smith et al. 2006), but also other models, that were compatible with the analysis of X-ray halos of other X-ray binaries (see, e.g., Smith 2008), gave good fits to our data. They resulted in distances for 1E 1547.0–5408 in the 4.8–5.4 kpc range. Other dust models giving relatively good fits imply distances of 6–8 kpc, but require that the highest peak seen in the CO emission corresponds to the cloud responsible for the second X-ray ring. This is not the brightest ring, and thus these scenarios would imply that the strength of the CO line is not proportional to the amount of dust that efficiently scatters X-rays.

We finally note that, if the X-ray source and dust distance are not independently constrained, the quality of the fits of the X-ray halo profiles is mostly sensitive to the grain size distribution in the range 0.01–0.03 μm, while the source distance is mainly determined by the largest grains. These grains, with size >0.1 μm, are those less constrained by diagnostics at longer wavelengths. Therefore, we cannot exclude that the actual dust properties may be different from all the models we tested, providing a good fit to the X-ray rings, but for a significantly different distance of 1E 1547.0–5408.

This research is based on observations with the NASA/UK/ASI *Swift* mission and with *XMM-Newton*, an ESA science mission with instruments and contributions directly funded by ESA Member States and NASA. We thank the *Swift* and *XMM-Newton* duty scientists and mission planners for making these target of opportunity observations possible. We thank T.M. Dame for granting us access to the CO emission data in the direction of 1E 1547.0–5408. We thank E. Bellm and J. Ripa for useful discussion of RHESSI results. We acknowledge the partial support from ASI (ASI/INAF contracts I/088/06/0 and AAE TH-058). PE thanks the Osio Sotto city council for support with a G. Petrocchi fellowship. SZ acknowledges support from STFC. NR is supported by a Ramón y Cajal fellowship. DG acknowledges the CNES for financial support.

Facilities: Swift (XRT), XMM-Newton (EPIC)

REFERENCES

Bellm, E., Smith, D. M., & Hurley, K. 2009, GCN Circ., 8857
Burrows, D. N., et al. 2005, Space Science Reviews, 120, 165
Camilo, F., Ransom, S. M., Halpern, J. P., & Reynolds, J. 2007, ApJ, 666, L93
Clemens, D. P. 1985, ApJ, 295, 422
Cordes J. M., Lazio T. J. W. 2002, eprint (astro-ph/0207156)
Dame, T. M., Hartmann, D., & Thaddeus, P. 2001, ApJ, 547, 792
Draine, B. T. 2003, ApJ, 598, 1026
Gelfand, J. D. & Gaensler, B. M. 2007, ApJ, 667, 1111

Halpern, J. P., Gotthelf, E. V., Reynolds, J., Ransom, S. M., & Camilo, F. 2008, ApJ, 676, 1178
Hurley, K., et al. 1999, Nature, 397, 41
Israel, G. L., et al. 2009, MNRAS, submitted
Marshall, D. J., Robin, A. C., Reylé, C., Schultheis, M., & Picaud, S. 2006, A&A, 453, 635
Mathis, J. S. & Lee, C.-W. 1991, ApJ, 376, 490
Mathis, J. S., Rumpl, W., & Nordsieck, K. H. 1977, ApJ, 217, 425
Mauche, C. W. & Gorenstein, P. 1986, ApJ, 302, 371
Mazets, E. P., Aptekar, R. L., Butterworth, P. S., Cline, T. L., Frederiks, D. D., Golenetskii, S. V., Hurley, K., & Il'Inskii, V. N. 1999, ApJ, 519, L151
Mazets, E. P., Golentskii, S. V., Ilinskii, V. N., Aptekar, R. L., & Guryan, I. A. 1979, Nature, 282, 587
Mereghetti, S. 2008, A&A Rev., 15, 225
Mereghetti, S., et al. ApJ, 696, L74
Moretti, A., et al. 2005, Proc. SPIE, 5898, 360
Overbeck, J. W. 1965, ApJ, 141, 864
Predehl, P., Burwitz, V., Paerels, F., & Trümper, J. 2000, A&A, 357, L25
Predehl, P. & Schmitt, J. H. M. M. 1995, A&A, 293, 889
Read, A. M. 2004, XMM-Newton Science Operations Centre, XMM-Newton CCF Release Note (Madrid, Spain), http://xmm2.esac.esa.int/docs/documents/CAL-SRN-0167-1-1.ps.gz
Rolf, D. P. 1983, Nature, 302, 46
Smith, R. K. 2008, ApJ, 681, 343
Smith, R. K., Dame, T. M., Costantini, E., & Predehl, P. 2006, ApJ, 648, 452
Smith, R. K. & Dwek, E. 1998, ApJ, 503, 831
Strüder, L., et al. 2001, A&A, 365, L18
Tiengo, A., Mereghetti, S., Vianello, G., Esposito, P., Israel, G. L., Rea, N., & Götz, D. 2009, GCN Circ., 8848
Trümper, J. & Schönfelder, V. 1973, A&A, 25, 445
Turner, M. J. L., et al. 2001, A&A, 365, L27
Valencic, L. A., Smith, R. K., Dwek, E., Graessle, D., & Dame, T. M. 2009, ApJ, 692, 502
Vaughan, S., et al. 2004, ApJ, 603, L5
Vianello, G., Tiengo, A., & Mereghetti, S. 2007, A&A, 473, 423
Vink, J. & Bamba, A. 2009, ApJ, 707, L148
Weingartner, J. C. & Draine, B. T. 2001, ApJ, 548, 296
Zubko, V., Dwek, E., & Arendt, R. G. 2004, ApJS, 152, 211